processes

MDPI

Article

Failure Analysis of Drill Pipe during Working Process in a Deep Well: A Case Study

Luchun Li [1,2,*], Zhanghua Lian [1,*] and Changhong Zhou [2]

[1] Petroleum Engineering School, Southwest Petroleum University, Chengdu 610500, China
[2] Drilling & Production Technology Research Institute, CNPC Chuanqing Drilling Engineering Company Limited, Guanghan 618300, China
* Correspondence: lilc_zcy@cnpc.com.cn (L.L.); milsu1964@163.com (Z.L.)

Abstract: The failure of a 101.6 mm drill pipe was studied by combining experimental testing and finite element simulation. The macro analysis, metallographic structure and energy spectrum, chemical composition and a mechanical property test of the failed drill pipe sample were firstly carried out. Then, a three-dimensional finite element model of drill pipe failure was established based on the experimental results. Finally, the failure mechanism of drill pipe was analyzed and the mitigation measures were put forward. The results showed that solids settling sticking was the direct cause of fracture failure of the drill pipe joint. Due to the violent friction and wear between the drill pipe joint and the settled sand, the large amount of heat generated caused the microstructure of the joint material to undergo phase transformation and the bearing capacity to be reduced. Finally, fracture occurs under tensile and torsional loads.

Keywords: deep well; drill pipe failure; gravel sedimentation; metal phase transition; friction

Citation: Li, L.; Lian, Z.; Zhou, C. Failure Analysis of Drill Pipe during Working Process in a Deep Well: A Case Study. *Processes* **2022**, *10*, 1765. https://doi.org/10.3390/pr10091765

Academic Editor: Raul D.S.G. Campilho

Received: 11 July 2022
Accepted: 26 August 2022
Published: 3 September 2022

1. Introduction

To meet the rapid growth of global energy consumption, ultra-high temperature and ultra-high pressure petroleum and gas wells have gradually attracted the attention of the industry. However, due to the complex downhole environment of such petroleum and gas wells, the stress of drill pipe is very complicated in the process of drilling [1,2]. Consequently, the failure of drill pipe often occurs in ultra-deep well drilling. In recent years, a large number of drill-pipe failures in ultra-deep wells have been reported, and serious drill pipe failures have occurred in some areas [3,4].

Many scholars have tried to explain the reasons behind the failure of drill pipe. Zamani et al. (2016) investigated numbers of past drill pipe research results and discussed all metallurgical and mechanical aspects of failure that can occur for a drill pipe. They argued that the foremost factors may be complex loading, combined stresses and different types of vibrations. In addition, they support that the fatigue crack is the root cause of drill-pipe failure [5]. Liu et al. (2015) analyzed the axial cracking failure in consideration of the service condition, material quality and stress corrosion mechanism systematically, proceeded measurement and inspection on macroscopic and microscopic morphology of crack surface, corrosion products and circumferential residual stress. Then, established the relationship between the erosion wear loss of drill pipe and drilling parameters such as gas injection volume and rate of penetration [6]. Huang et al. (2017) built a drill-pipe erosion experiment model based on the micro-cutting model of single rock particle. Their test results show that the gas-injection volume has more impact on drill-pipe erosion compared to the rate of penetration, and a high rate of penetration will suppress the erosion wear of drill pipe [7]. Abdo et al. (2017) considered that the main reason causing drill pipes failure is fatigue due to vibration. Hence, a novel in-house experimental setup has been developed to mimic downhole axial, lateral and torsional vibration modes and mechanisms in drilling operations, and investigate the drill-pipe fatigue failure due to cyclic stresses,

on account of the research deficiency of quantitative assessment methods of drill-pipe fatigue [8]. Luo et al. (2020) provided a modified model for the S-N data, revealing the correlation between the fatigue life and fatigue limit, equivalent stress amplitude reflecting the effect of stress ratio to predict the fatigue damage of drill-pipe. The research shows that the mechanism of the fatigue fracture was examined by scanning electron microscopy [9]. Zhang et al. (2020) analyzed the chemical composition, mechanical properties and microstructures of the failed drill-pipe materials by experiments. Then used the finite element method to investigate the static stress characteristics and fatigue life of the drill pipe joint under multi-axial alternating loads and found that the alternating load was the main factor of failure [10]. Ahmed et al. (2020) investigated a twisted-off failure specimen of heavy weight drill pipe (HWDP) though macro and micro tests. Their research showed that the HWDP failed by a corrosion fatigue mechanism [11].

Since 2021, drill-pipe failures have been reported more frequently. Liu et al. (2021) analyzed the failure of aluminum alloy drill pipe and studied the formation of pits and horizontal cracks on the surface of the drill pipe. They came to the conclusion that the cause of failure of aluminum alloy drill pipe is mainly attributed to the brittleness sensitivity of intermittent-banded second phase and inclusions to corrosive media from a muddy environment [12]. Yu et al. (2022) investigated the failure of S135 steel drill pipe and thought that the crack originated from the corrosion pit on the inner wall because of stress concentration, and extended along the circumference during the operation of lifting drill pipe for many times, and finally led to sudden fracturing [13]. Liu et al. (2022) studied the first titanium alloy drill-pipe failure accident, which occurred during the drilling of an ultra-short radius horizontal well in China; the results revealed that there are many micro-cracks on the surface of titanium alloy drill pipes that cannot be detected according to the current standards; when the titanium alloy drill pipe was used under the ultra-short radius horizontal drilling condition, the pipe body had slight deformation and these micro-cracks rapidly expanded throughout the entire wall thickness, resulting in the fracture failure [14].

According to the literature, previous studies have summarized the causes of drill pipe failure as fatigue, corrosion, erosion, vibration, and stress concentration. Drill pipe failure is highly uncertain and difficult to predict. Although many scholars have undertaken a lot of research on drill pipe failure, it is still frequently reported. Recently, a drill pipe failure occurred during an unstuck operation, in order to find the reason for the fractured drill pipe. This paper used the experimental methods including macroscopic analysis, metallographic structure and energy spectrum analysis, chemical composition analysis and mechanical property analysis, combined with 3D drill pipe-sedimentary gravel thermal stress coupled finite element model, studied the failure mechanism of drill pipe caused by sedimentary gravel sticking. The measures to avoid the failure of drill pipe in field drilling operation are put forward. The research is of great significance to drill pipe protection and field operation safety.

2. Failure Case

The fracture failure accident of 101.6 mm drill pipe occurred in a certain well during drilling operation. The morphology of the failed drill pipe sample was shown in Figure 1a. The distance between the joint torque shoulder surface and the fracture position is about 265 mm; the distance between the torque shoulder surface and the slope shoulder of 35° is about 212 mm, and; the outer diameter of the drill pipe joint is 132.8 mm. The shoulder chamfering diameter is 127.48 mm and the inner diameter is 61.5 mm. The side of the tube body at the fracture is bright white with obvious friction marks. The outer diameter at the fracture is about 79.4 mm, the inner diameter is about 64.8 mm, the outer diameter of the tube body is about 101.8 mm, and the outer diameter of the thickening part of the tube body is about 105.5 mm. Friction and wear marks on the 35° slope shoulder of the drill pipe joint are evident with some hard adhesives attached. There are also obvious friction and wear phenomena at the drill pipe joint body, and there are many mud erosion marks (Figure 1b,c) on the outer surface circumference near the arc groove. It is worth noting that

some tongs indentation was indeed found on the failed drill pipe joint, but these bite marks were shallow and did not affect the structural integrity and strength of the joint, and no obvious bite marks were found at the fracture position of the failed drill pipe. Therefore, the indentation caused by the fit out and disassembly of the joint is not the main cause of this failure. In addition, when the failed sample was cut open as displayed in Figure 2, the inner wall of the sample near the fracture showed obvious marks of high-temperature burning, and the coating was seriously discolored and fell off.

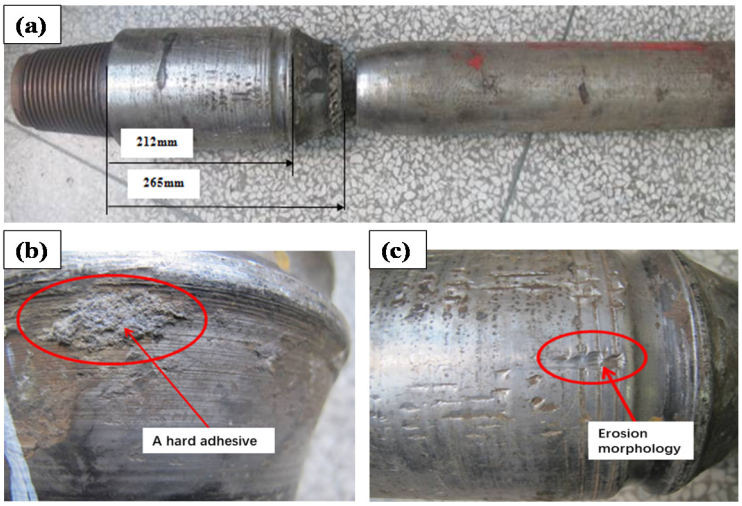

Figure 1. Macro morphology of failed drill pipe sample, (**a**) Macro topography of failed drill pipe; (**b**) Hard adhesive; (**c**) Erosion morphology.

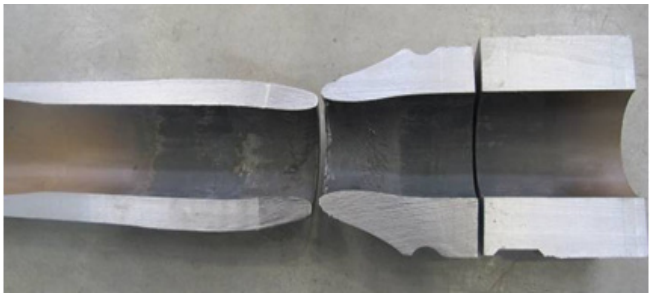

Figure 2. Damage morphology of coating on inner wall of failed drill pipe.

3. Experimental Process

3.1. Metallographic Structure and Energy Spectrum Analysis

After sampling and cleaning the failed drill pipe, it was found that the fracture was located at the joint body approximately 36.4 mm from the weld. There are two distinct thermal effect boundaries symmetrically distributed on both sides of the fracture surface of the sample, which are consistent with the trace line of the discoloration position of the inner coating. Figure 3 shows the partition and numbering of the failed samples, it is clear that there is necking phenomenon due to tensile yield in zone A and zone E. Figure 4 demonstrates the analysis results of metallographic structure in different zones, it can be seen from Figure 4 that there are a lot of martensite and bainite and tempered sorbite in the material near the fracture. However, with the increase in the distance from the fracture, the content of martensite decreases and the tempered soxtensite increases. Figure 5 shows the hardness test results of the failed sample; it can be seen that the hardness of the material near the fracture is obviously higher than that far away from the fracture.

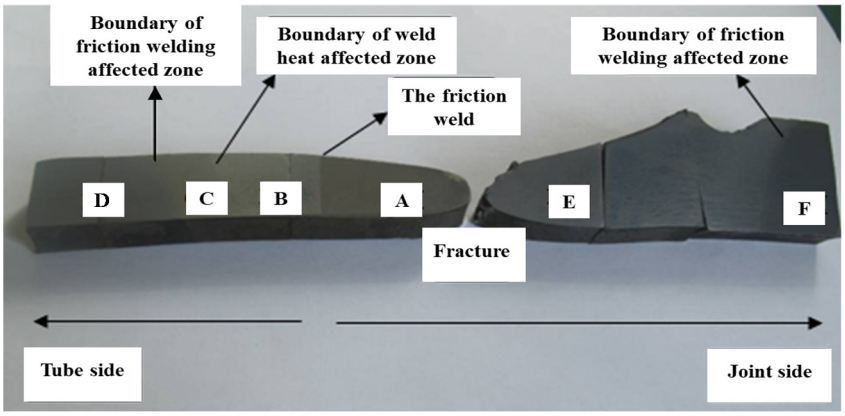

Figure 3. Sectional partition of failed sample.

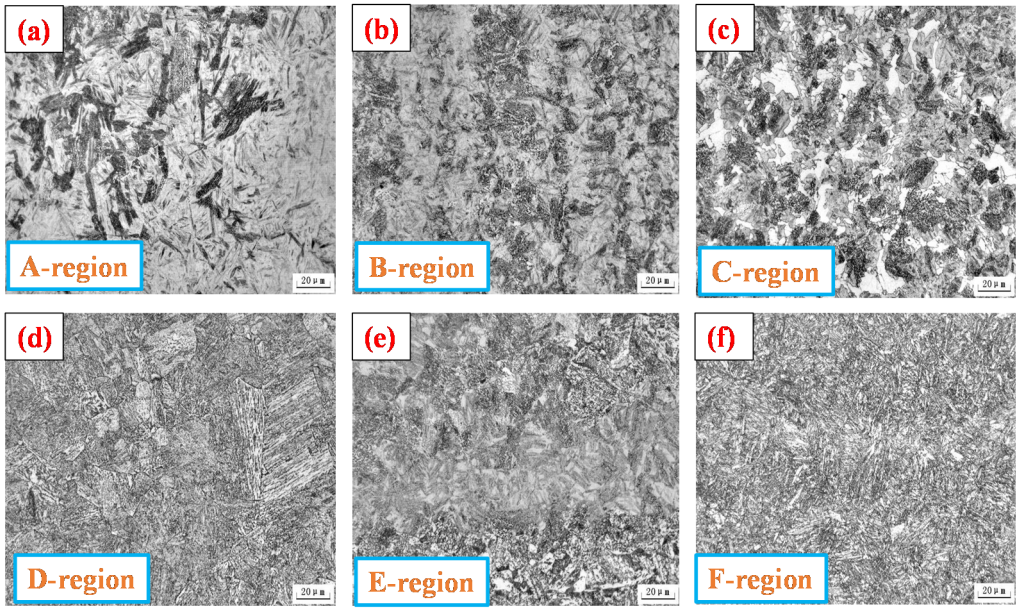

Figure 4. Metallographic structure analysis results.

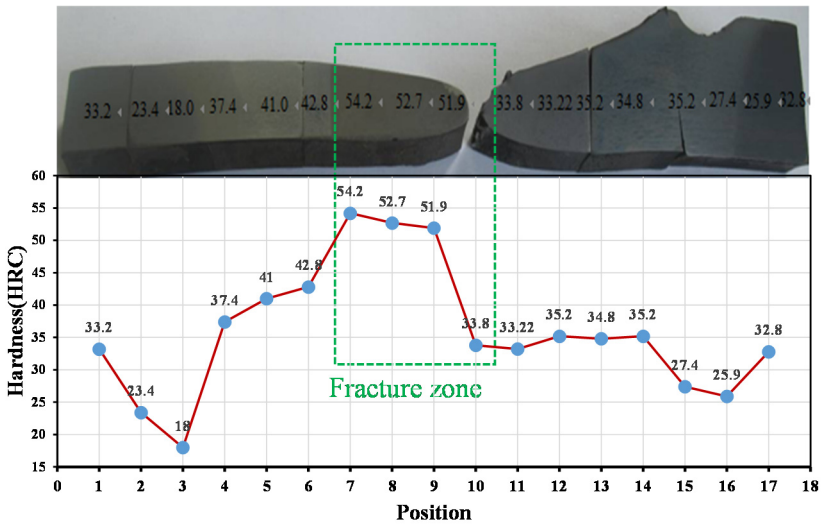

Figure 5. Variation in hardness on the sample section.

Energy spectrum analysis was performed near the fracture, as shown in Figure 6. It is clear that there are many black adhesives near the joint and a large number of white particles on the surface of the matrix. The main components of the black adhesive are Si and O, as well as some elements such as Ca and Na. The main components of the white particles in the adhesive are Fe and O. It can be concluded that the black adhesive is mainly silicon dioxide and silicate, and the white particles in the adhesive are the peeling metal particles and corrosion products on the drill pipe joint matrix.

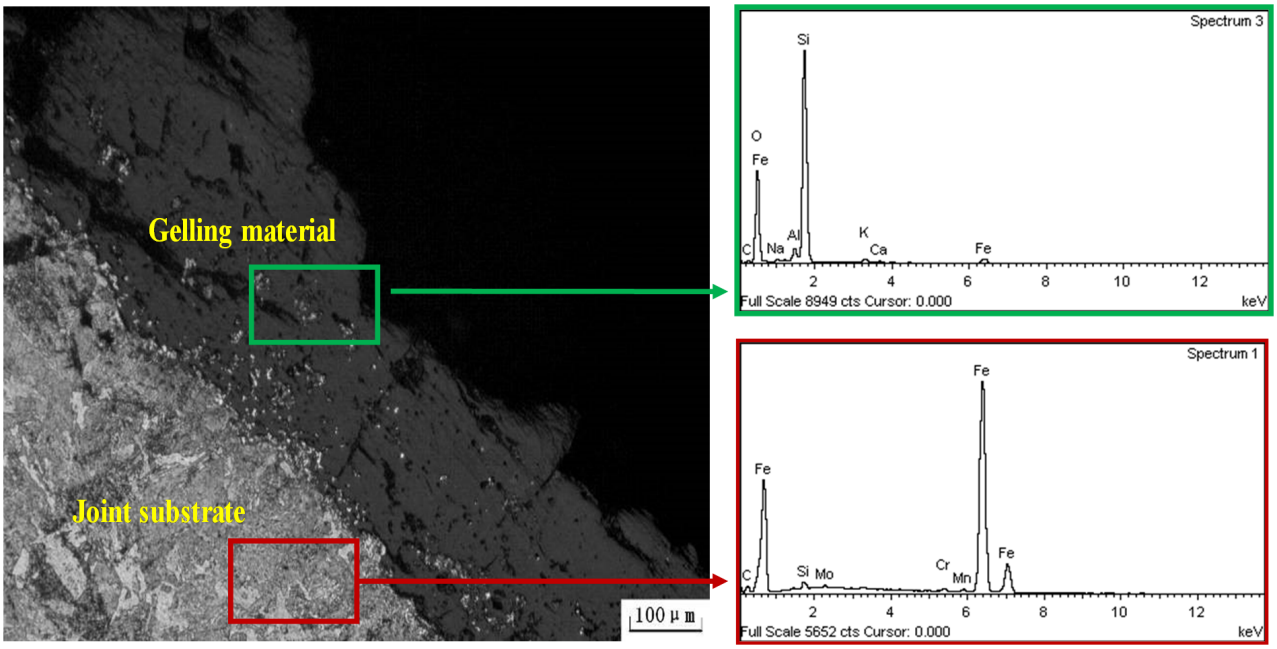

Figure 6. Energy spectrum analysis results of fracture location.

3.2. Chemical Composition Analysis

Table 1 lists the chemical composition analysis results of failed drill pipe joint, the content of S and P in the chemical composition of the drill pipe joint conforms to API Spec 5DP-2010 and SY/T 5561. Therefore, chemical composition is not the cause of failure.

Table 1. Drill pipe joint chemical composition test results (wt, %).

Elements	C	Si	Mn	P	S	Cr	Mo	Ni
Content	0.37	0.25	0.94	0.0092	0.0031	1.12	0.30	0.11
API Spec 5DP-2010	/	/	/	≤0.020	≤0.015	/	/	/
SY/T 5561	/	/	/	≤0.020	≤0.015	/	/	/

3.3. Mechanical Properties Tests

The 12.7 mm diameter round-rod tensile sample, the 10 × 10 × 55 mm longitudinal Charpy V-notch impact sample and hardness sample were taken from the failed drill pipe joint sample far from the fracture. The test results are shown in Figure 7 and Table 2. The results show that the tensile properties, longitudinal impact energy and hardness of the failed drill-pipe joint meet the requirements of API Spec 5DP-2010 and SY/T 5561. Therefore, there is no quality problem of the joint leading to the accident.

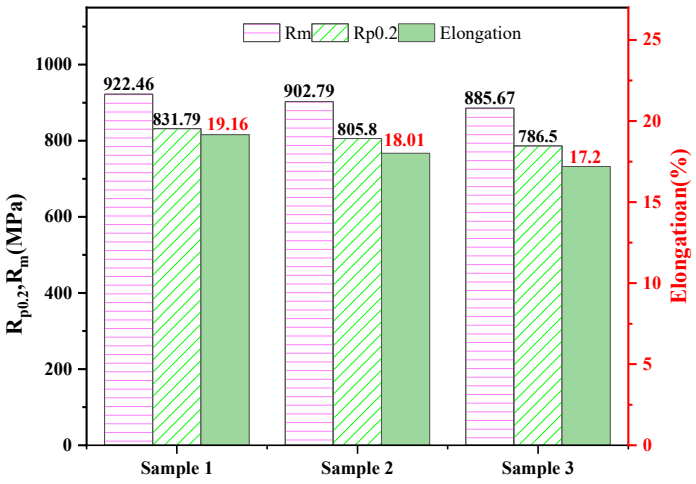

Figure 7. Tensile results of drill pipe specimens.

Table 2. Mechanical properties of drill pipe joint.

Test Item	Yield Strength (MPa)	Tensile Strength (MPa)	Extend Rate (%)	Impact Energy/−20° C (J)	Section Hardness (HB)	Surface Hardness (HB)
Single value	931 944 956	1066 1051 1079	19.1 18.3 16.9	108 119 106	314 320 316	311 311 309
Mean value	943	1065	18.1	111	317	310
API Spec 5DP-2010	827~1138	≥965	≥13	Mean value ≥ 54 Single value ≥ 47	285~341	/
SY/T5561	≥827	≥965	≥13	Mean value ≥ 70 Single value ≥ 61	≥285	285~341

4. Modeling

Based on the real size and failure condition of drill pipe mentioned in the failure case, a drill pipe and sedimentary gravel model in contact with drill pipe were established, forming a stress-temperature coupling three-dimensional (3D) finite element model. The 3D model, including the solid model is presented in Figure 8a, and the axial section view is shown in Figure 8b.

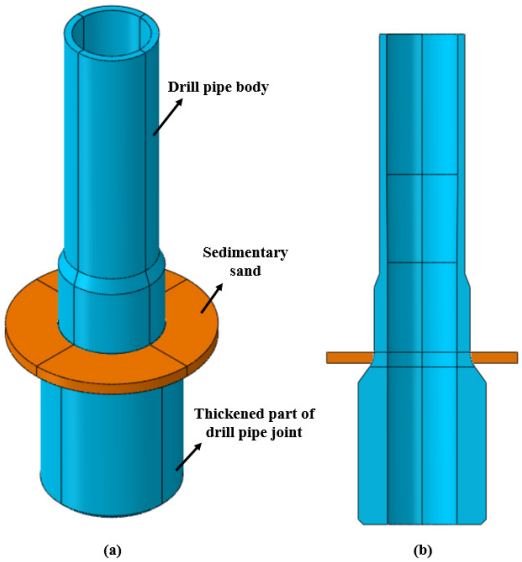

Figure 8. Structure size of drill pipe and 3D drill pipe-gravel solid model.

The solid model was meshed. To make the simulation calculation results more accurate, secondary mesh encryption was carried out in the friction welding area where drill pipe and gravel contact as shown in Figure 9. The drill-pipe material is S135 steel; the mechanical and thermodynamic properties, referring to the mechanical performance test results, are shown in 3.3 above. Meanwhile, the properties of the sedimentary gravel material properties are shown in Table 3. The friction coefficient between drill pipe and gravel particles is set to 0.35.

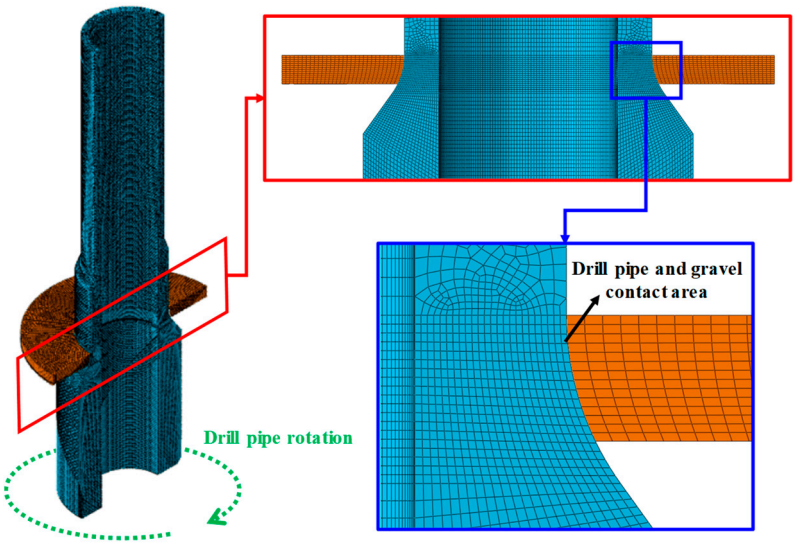

Figure 9. Model meshing and encryption of drill-pipe gravel contact area.

Table 3. Parameters of sedimentary gravel materials.

Density (kg/m^3)	Elasticity Modulus (MPa)	Poisson's Ratio	Compressive Strength (MPa)	Tensile Strength (MPa)	Cohesion Strength (MPa)	Friction Angle (°)
2530	14.7	0.36	143	2.6	27.2	27.8

The core of solving the transient temperature field problem is to use the corresponding numerical method to solve the linear ordinary differential equations. By deducing the governing equation of the three-dimensional transient temperature field in classical thermodynamics, the linear ordinary differential equations with time $\boldsymbol{t}$ as the independent variable can be obtained [15,16].

$$C\dot{\phi} + K\phi = P \tag{1}$$

where, C is the heat capacity matrix; $\dot{\phi}$ is the derivative array of node temperature with respect to time; K is the heat conduction matrix; ϕ is node temperature array; P is the temperature load array.

The elements of matrix C, K and P are integrated by the corresponding matrix elements of the element, as follows:

$$K_{ij} = \sum_e \int_{\Gamma_3^e} hN_iN_jd\Gamma + \sum_e \int_{\Omega^e} \left(k_x \frac{\partial N_i}{\partial x}\frac{\partial N_j}{\partial x} + k_y \frac{\partial N_i}{\partial y}\frac{\partial N_j}{\partial y} + k_z \frac{\partial N_i}{\partial z}\frac{\partial N_j}{\partial z} \right) d\Omega \tag{2}$$

$$C_{ij} = \sum_e \int_{\Gamma_3^e} \rho cN_iN_jd\Gamma \tag{3}$$

$$P_i = \sum_e \int_{\Omega^e} \rho QN_iN_jd\Omega + \sum_e \int_{\Gamma_3^e} qN_id\Gamma + \sum_e \int_{\Gamma_3^e} h\phi_a N_id\Gamma \tag{4}$$

By means of the above equation, the partial differential equation problem in time domain and space domain can be transformed into the initial value problem of the ordinary differential equation of temperature $\phi_i(t)$ with N nodes in space domain.

Thermal stress is the result of the interaction of temperature field and stress field. The interaction of temperature field and stress field is called thermal-solid coupling problem. The finite element equation calculated by thermo-structure analysis is:

$$\begin{pmatrix} M & 0 \\ 0 & 0 \end{pmatrix} \begin{pmatrix} \ddot{u} \\ \ddot{T} \end{pmatrix} \begin{pmatrix} C & 0 \\ 0 & C_t \end{pmatrix} \begin{pmatrix} \dot{u} \\ \dot{T} \end{pmatrix} + \begin{pmatrix} K & 0 \\ 0 & K_t \end{pmatrix} \begin{pmatrix} u \\ T \end{pmatrix} = \begin{pmatrix} F \\ Q \end{pmatrix} \quad (5)$$

where, M is the mass matrix; u and T are displacement and temperature load, respectively. C is structural damping matrix; C_t is specific heat matrix; K is the structure stiffness matrix; K_t is the heat conduction matrix; F is the total equivalent nodal force array; Q is the total equivalent node heat flux vector [17].

5. Results and Discussion

In the actual drilling operation, according to the 5530 m depth of wellbore, the hydrostatic pressure of drill pipe environment can be calculated as 81.3 MPa. Due to the obvious pressure drop of drilling fluid during the process of drilling fluid passing through the drill bit and then returning from the wellbore, the internal pressure of drill pipe can be calculated as 92.8 MPa according to Bernoulli equation. At the same time, the drill pipe is subjected to axial loads from the upper drill pipe and the formation. When the drill pipe rotates, the sedimentary gravel in the wellbore will rub against the friction welding area of the drill-pipe joint, resulting in friction heat, changing the thermal stress of the drill pipe material, resulting in metal phase transformation, reducing the strength of the drill pipe, and ultimately leading to fracture failure of the drill pipe. When the drill pipe rotation speed is 60 rpm, the temperature-distribution contour diagram of the friction area between the drill pipe and gravel advancing over time is shown in Figure 10. It can be seen that the highest temperature occurs in the friction welding area of drill pipe where the outer wall of drill pipe is in contact with the sedimentary gravel, and gradually decreases to both ends, and the maximum temperature of the outer wall of drill pipe reaches 838 °C. At the same time, the lowest temperature was found at both ends of the drill pipe, with a minimum temperature of 20 °C. The temperature change of the outer wall of the drill pipe follows the following steps: ***(i)*** At the initial stage of friction, a high temperature zone is generated at the contact area between the outer wall of the drill pipe and the gravel, but the temperature change does not extend across the drill pipe; ***(ii)*** As time goes on, the temperature in the friction region further increases and the temperature variation region expands, but the high temperature region becomes more concentrated; ***(iii)*** Later, the high temperature zone also began to expand, and the temperature variation zone extended to a larger area of the drill pipe. From the analysis of the temperature level and distribution with time, it can be seen that at the beginning of the contact friction between the drill pipe and gravel, the temperature of the outer wall of drill pipe begins to rise due to the heat generated by friction. Subsequently, due to the cooling effect of the drilling fluid, the hot zone on the drill pipe began to be concentrated in the friction area, and the temperature continuously spread across the drill pipe. Finally, as the temperature increases, the entire temperature range expands across the drill pipe.

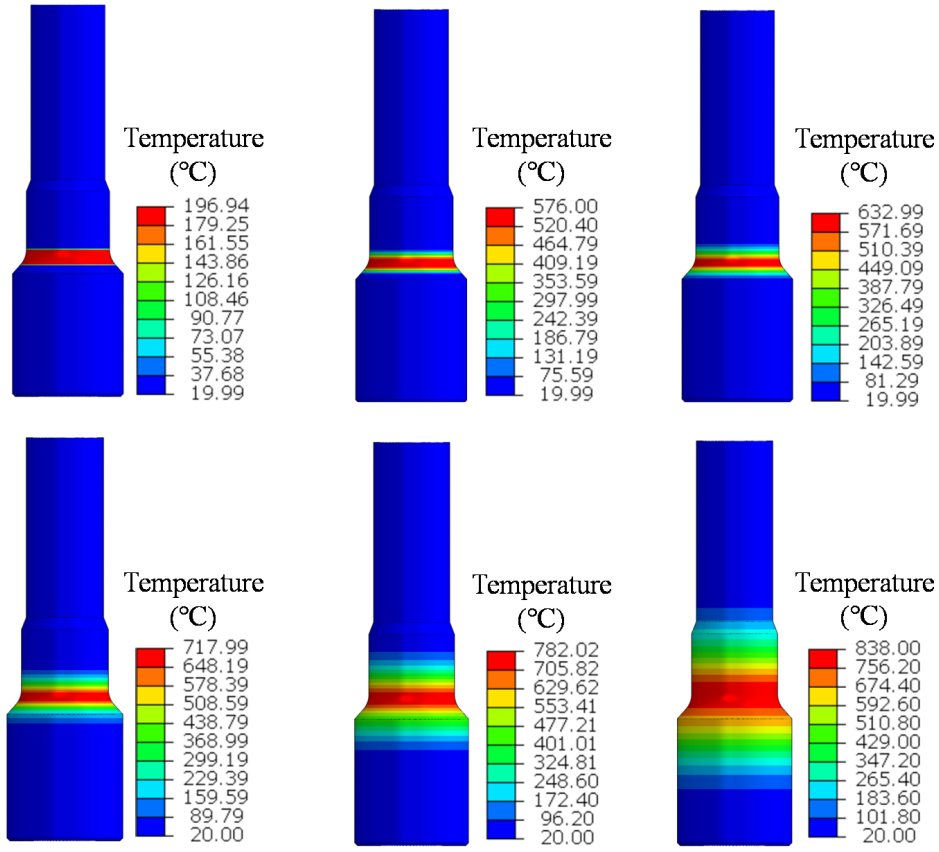

Figure 10. Temperature distribution contour of drill pipe outer wall at different time.

However, the variation in temperature level and distribution along the direction of drill-pipe wall thickness has a great influence on the strength of drill pipe material. Figure 11 shows the temperature level and distribution of drill pipe along the wall thickness direction under the condition of a well depth of 5530 m and a drill pipe rotation speed of 60 rpm. It can be seen that the temperature-expansion process on the drill pipe axis is the same as that on the outer wall, while the temperature change process on the drill pipe wall thickness direction follows the following steps: ***(i)*** When the friction between drill pipe and gravel begins, the temperature increases in the thinner area of drill pipe wall thickness; ***(ii)*** Subsequently, the zone of temperature variation begins to expand into the drill pipe along the wall thickness until the high temperature zone completely passes through the drill pipe wall thickness; ***(iii)*** After the hot zone passes through the drill pipe wall thickness, it begins to extend axially along the drill pipe. From this process analysis, it can be seen that in the direction of the drill-pipe wall thickness, the high-temperature zone firstly expands from the outside to the inside, and gradually reduces the material strength of the whole drill-pipe wall thickness, and then expands along the drill-pipe axial direction, and the reduction range of material strength becomes larger.

The axial temperature distribution curves of the outer and inner walls of the drill pipe were extracted by defining paths from top to bottom along the inner and outer walls of drill pipe, respectively. Figure 12 displays the temperature distribution of the outer wall of the drill pipe at different times. It can be seen that as time goes on, the maximum temperature on the drill pipe becomes higher and higher. In the initial friction, the temperature changes only in the contact area, and then gradually spreads to the whole friction welding area and even other areas. After 60 min of friction between the drill pipe and the gravel, the highest temperature on the outer wall of the drill pipe reached 838 °C.

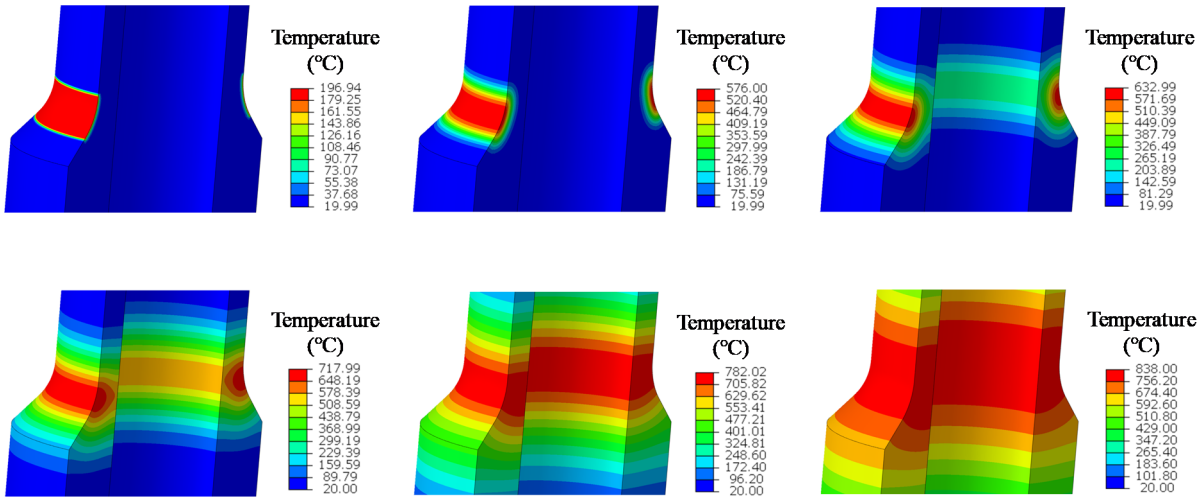

Figure 11. Distribution contour of temperature in the direction of drill pipe wall thickness at different times.

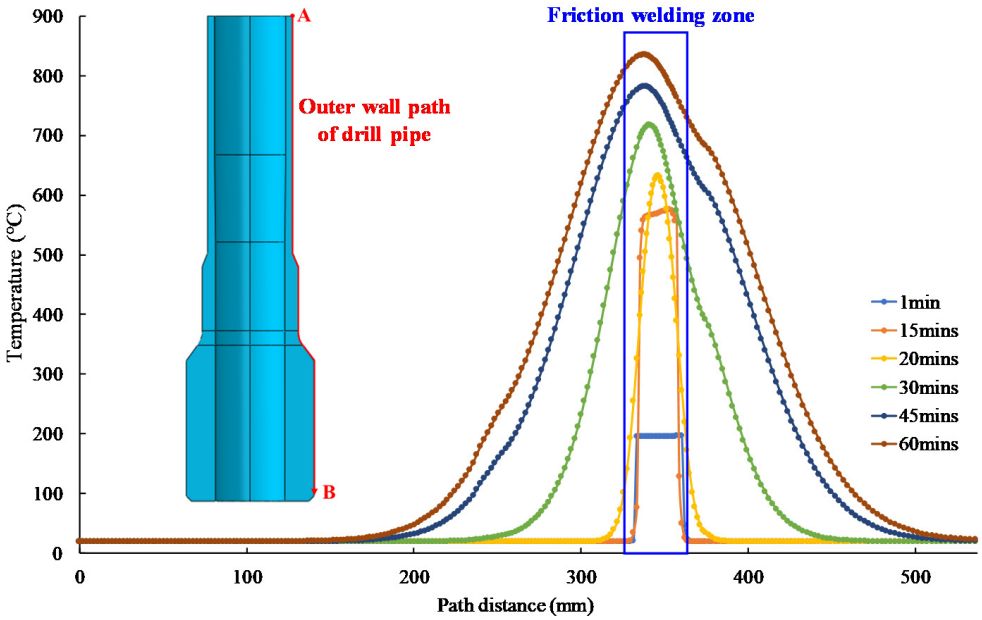

Figure 12. Temperature variation curves at different times along the outer path of drill pipe.

Figure 13 displays the internal temperature distribution of the drill pipe at different times. It is clear that when the friction time between drill pipe and sedimentary gravel is less than 15 min; the friction heat generated on the outer wall of drill pipe does not pass through the thickness of drill pipe wall, so there is no temperature change in the inner wall of drill pipe. Then, as time goes on, the temperature inside the drill pipe gradually increases and the range of temperature changes gradually increases, with the highest temperature appearing in the friction welding area and even extending to the area outside the contact zone. When the friction time reaches 60 min, the maximum internal temperature of the drill pipe reaches 836 °C, which is very close to the external temperature of the drill pipe. Hence, the law can be obtained to know that in the actual drilling process, if there is sand settling in the wellbore, the on-site operation should control the drilling time of each drill-pipe rotation. On the one hand, it can avoid the high temperature caused by the long time friction between drill pipe and gravel, resulting in the phase transition of drill pipe material and reduce the strength of drill pipe. On the other hand, it can avoid the high temperature

of the outer wall of drill pipe penetrating the wall thickness of drill pipe, resulting in the overall strength of the friction welding area of drill pipe, or even fusing the drill pipe.

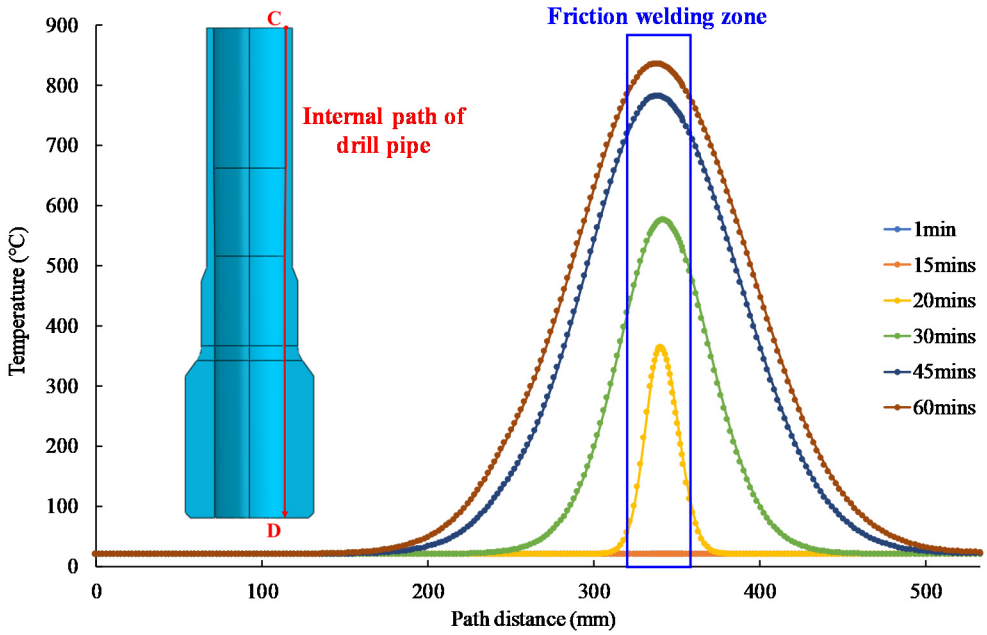

Figure 13. Temperature variation curves at different times along the inner wall path of drill pipe.

As a factor that can be controlled in the actual drilling process, the rotational speed also has a great influence on the heat generated by the friction between the friction welding area of the drill pipe and gravel deposited in the wellbore. By controlling the drilling speed of the drill pipe in the finite element model, the friction heat generation between the drill pipe and the gravel was simulated under different rotation speed conditions. The relationship between the maximum temperature on the drill pipe and the variation in rotational speed is shown in Figure 14. The process of increasing the maximum temperature on drill pipe can be divided into two stages: ***(i)*** When the drill pipe speed is lower than 50 rpm, the maximum temperature on the drill pipe increases with the increase in the rotation speed rapidly. For example, when the drill pipe speed is 30 rpm, the maximum temperature on the drill pipe is 684 °C, while when the drill pipe speed is 50 rpm, the maximum temperature is 816 °C; ***(ii)*** When the drill pipe rotation speed is higher than 50 rpm, the increasing trend of the maximum temperature on the drill pipe gradually becomes slow. When the drill pipe rotation speed is 100 rpm, the maximum temperature is 847 °C, compare with the maximum temperature under the condition of 50 rpm, the increase is slight. Therefore, it can be seen from the analysis of the law that, in the actual underground drilling process, if sand and gravel deposition occurs in the wellbore, the rotational speed of the drill pipe can be artificially controlled to avoid the phase transition of metal and the reduction of strength of the drill pipe caused by the high friction temperature. Based on the results of this study, we recommend that the rate of penetration should be artificially controlled at around 50 rpm during drilling. At the same time, it is recommended that the drilling time should not exceed 60 min, and switching the drill pipe in time and cooling down. Meanwhile, keeping a clean hole and drilling fluid circulation are effective measures to prevent such failure.

The fracture process of the failed drill pipe can be deduced by experiment and finite element analysis: First, during the operation, a large amount of cuttings accumulated on top of the failed drill-pipe external threaded joint due to poor wellbore stability. Under the pressure of the upper mud, the accumulated cuttings gradually compacted, blocking the mud circulation channel. Secondly, during the rotation and lifting operation, there is severe friction and wear between the joint and the cuttings. Due to the lack of mud cooling

and lubrication, a lot of friction heat is generated, which makes the local temperature of the contact part rise rapidly, austenitizing occurs in the structure of drill pipe material, the strength of material matrix decreases greatly, and the outer diameter and wall thickness decrease continuously. Finally, under the action of tensile, torsion and other composite loads, the material at high temperature will yield deformation and fracture.

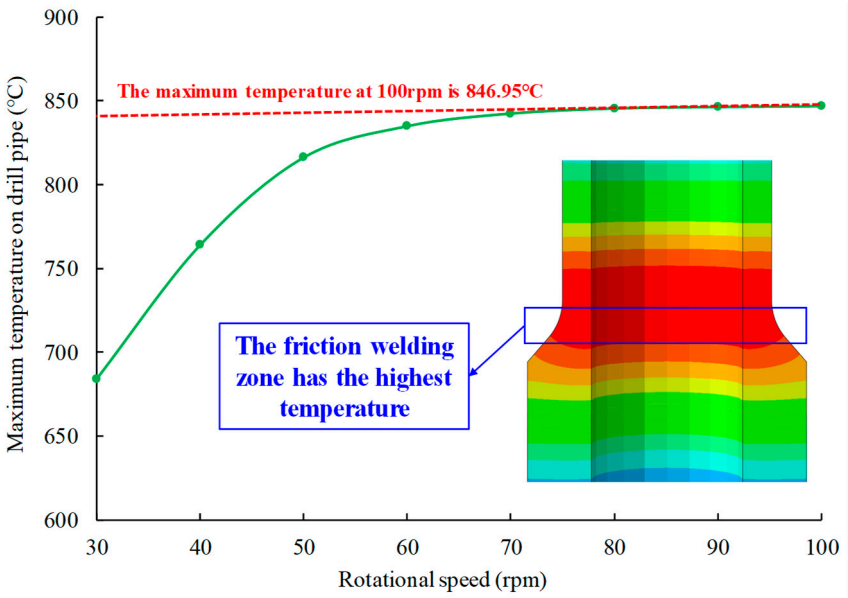

Figure 14. The relation curve between the maximum temperature and the rotational speed of drill pipe.

6. Conclusions

Based on the test results, including macroscopic analysis, metallographic structure and energy spectrum analysis, chemical composition analysis, and mechanical performance test for the friction welding area of 101.6 mm drill-pipe joints, combined with the use of finite element analysis method, a 3D drill pipe-sedimentary gravel thermal stress coupling model was established, and the friction and heat generation of the drill pipe and the sand were analyzed. The following conclusions were derived:

(1) The fracture failure of the drill pipe is due to the violent friction and wear of the drill pipe joint and the gravel, which leads to the reduction of the effective section of the failed part. The large amount of heat generated by the friction of the lack of mud cooling and lubrication makes the joint material organization phase change, and the bearing capacity further decreases, and eventually break under tensile and torsional loads.

(2) A large amount of cuttings accumulated on the 35° slope shoulder surface of the drill-pipe external threaded joint caused the sand-set stuck drill, which is an important reason for the fracture failure of the drill pipe joint.

(3) The occurrence of the maximum temperature on the drill pipe is related to the length of friction between the drill pipe and gravel and the speed of the drill pipe. The longer the friction time or the higher the drill pipe rotation speed, the higher the drill pipe temperature and the greater the influence range of temperature change.

(4) In order to avoid similar accidents happening again, the deposition of sand and gravel should be cleaned up, or the length of each drilling should be controlled and the drilling rate should be appropriately reduced while ensuring the drilling efficiency.

Author Contributions: Funding acquisition, Z.L.; investigation, Z.L.; methodology, C.Z.; project administration, C.Z.; software, Z.L.; validation, Z.L.; writing—original draft, L.L.; writing—review & editing, L.L. All authors have read and agreed to the published version of the manuscript.

Funding: The authors are grateful to the support from the National Natural Science Foundation of China (No. 51974271).

Institutional Review Board Statement: Not applicable.

Informed Consent Statement: Not applicable.

Data Availability Statement: Not applicable.

Acknowledgments: Thank Southwest Petroleum University for the support of the project experimental equipment. Thank Chuanqing Drilling Company for supporting the experimental materials of the project.

Conflicts of Interest: All data in the article come from the author, without plagiarism and copyright issues.

References

1. Yu, H.; Peng, X.; Lian, Z.; Zhang, Q.; Shi, T.; Wang, J.; Zhao, Z. Experimental and numerical simulation of fatigue corrosion behavior of V150 high-strength drill pipe in air and H_2S-dilling mud environment. *J. Nat. Gas Sci. Eng.* **2021**, *98*, 104392. [CrossRef]
2. Peng, X.; Yu, H.; Lian, Z.; Dong, B.; Zhong, W.; Zhang, Y.; Hu, Z. Material optimization of drill pipe in complex wellbore environments by comparing fatigue life and cost. *Energy Rep.* **2021**, *7*, 5420–5430. [CrossRef]
3. Peng, X.; Yu, H.; Lian, Z.; Zhang, Q. Experimental and theoretical study on the mechanical properties of titanium alloy drill pipe in short radius and long horizontal wells. *J. Braz. Soc. Mech. Sci. Eng.* **2021**, *43*, 1–13. [CrossRef]
4. Zeng, D.; Dong, B.; Zeng, F.; Yu, Z.; Zeng, W.; Guo, Y.; Peng, Z.; Tao, Y. Analysis of corrosion failure and materials selection for CO_2–H_2S gas well. *J. Nat. Gas Sci. Eng.* **2020**, *86*, 103734. [CrossRef]
5. Zamani, S.M.; Hassanzadeh-Tabrizi, S.A.; Sharifi, H. Failure analysis of drill pipe: A review. *Eng. Fail. Anal.* **2016**, *59*, 605–623. [CrossRef]
6. Liu, Y.; Lian, Z.; Lin, T.; Shen, Y.; Zhang, Q. A study on axial cracking failure of drill pipe body. *Eng. Fail. Anal.* **2016**, *59*, 434–443. [CrossRef]
7. Huang, Z.; Xie, D.; Huang, X.; Li, G.; Xie, S. Analytical and experimental research on erosion wear law of drill pipe in gas drilling. *Eng. Fail. Anal.* **2017**, *79*, 615–624. [CrossRef]
8. Abdo, J.; Hassan, E.; Al-Shabibi, A.; Kwak, J. Design of a Testing Facility for Investigation of Drill Pipes Fatigue Failure. *J. Eng. Res.* **2017**, *14*, 105–114. [CrossRef]
9. Luo, S.; Liu, M.; Zheng, X. Characteristics and life expression of fatigue fracture of G105 and S135 drill pipe steels for API grade. *Eng. Fail. Anal.* **2020**, *116*, 104705. [CrossRef]
10. Zhang, Z.; Zhu, X. Failure analysis and improvement measures of step transition zone of drill pipe joint. *Eng. Fail. Anal.* **2019**, *109*, 104211. [CrossRef]
11. Ahmed, M.; El-Zomor, M.; Khafagi, S.; El-Helaly, M. Metallurgical failure analysis of twisted-off heavy weight drillpipe. *Eng. Fail. Anal.* **2020**, *112*, 104531. [CrossRef]
12. Liu, W.; Li, J.; Zhong, Y.; Shi, T.; Zhang, J.; Li, S. Failure analysis on aluminum alloy drill pipe with pits and parallel transverse cracks. *Eng. Fail. Anal.* **2021**, *131*, 105809. [CrossRef]
13. Yu, Z.; Zeng, D.; Hu, S.; Zhou, X.; Lu, W.; Luo, J.; Fan, Y.; Meng, K. The failure patterns and analysis process of drill pipes in oil and gas well: A case study of fracture S135 drill pipe. *Eng. Fail. Anal.* **2022**, *138*, 106171. [CrossRef]
14. Liu, Q.; Tong, K.; Zhu, G.; Tan, Y.; Zhang, J.; Xu, X.; Li, X.; Song, S. Investigation of fracture causes of the titanium alloy drill pipe in ultra-short radius horizontal well drilling. *Eng. Fail. Anal.* **2022**, *140*, 106516. [CrossRef]
15. Kryzhanivskyi, E.I.; Nykyforchyn, H.M.; Student, O.Z.; Krechkovska, H.V.; Chudyk, I.I. Role of Nonmetallic Inclusions in Premature Stress-Corrosion Fractures of Drill Pipes. *Mater. Sci.* **2020**, *55*, 822–830. [CrossRef]
16. Lv, D.; Zhang, T.; Gong, F. Study on Properties of Cold-Sprayed Al-Zn Coating on S135 Drill Pipe Steel. *Adv. Mater. Sci. Eng.* **2020**, *2020*, 1–10. [CrossRef]
17. Wu, C.; Kong, F.; Zhou, X. Numerical simulation of thermosetting coupling characteristics of equipment gate under marine environment. *Press. Vessel. Technol.* **2021**, *38*, 40–48.